Analysis of a New Modular E-type Consequent Pole Flux Reversal Motor

Mohammad Reza Sarshar
Department of Electrical Engineering
Amirkabir University of Technology
(Tehran Polytechnic)
Tehran, Iran
rezasarshar@aut.ac.ir

Mohammad Amin Jalali Kondelaji
e-Motion and APL Labs
Mechanical Engineering Department
University College London (UCL)
London, UK
amin.jalali@ucl.ac.uk

Pedram Asef
e-Motion and APL Labs
Mechanical Engineering Department
University College London (UCL)
London, UK
pedram.asef@ucl.ac.uk

Mojtaba Mirsalim
Department of Electrical Engineering
Amirkabir University of Technology
(Tehran Polytechnic)
Tehran, Iran
mirsalim@aut.ac.ir

***Abstract*—This paper proposes a novel modular consequent pole flux reversal permanent magnet (CPFRM) motor, which improves air-gap flux density and enhances performance under both no-load and full-load conditions. The improvement in air gap flux is demonstrated through a simplified magnetic equivalent circuit (MEC) in comparison with a conventional flux reversal motor (FRM). Furthermore, the proposed CPFRM is optimized using a genetic algorithm (GA) to maximize average torque while minimizing torque ripple. Performance enhancements over conventional motors are analyzed using finite element analysis (FEA) under no-load, full-load, and overload conditions. FEA results validate the superiority of the proposed motor, showing a 33.3% and 7.1% increase in full-load torque compared to flux-switching and flux-reversal PM motors, respectively. Additionally, the motor prototyping procedure is described in detail. A comprehensive conclusion summarizes the key findings.**

***Index Terms*—Consequent pole, flux reversal motor, stator-PM motor, magnetic equivalent circuit, finite element analysis**

I. Introduction

Embedding permanent magnets (PMs) in electric motors significantly enhances torque density, making them well-suited for electric vehicle (EV) applications [1], [2]. PMs can be embedded either in the stator or the rotor. Most conventional PM machines are rotor-based, such as surface-mounted permanent magnet (SPM) motors [3]. However, rotor-mounted PMs are subjected to severe centrifugal forces and vibrations, which can lead to the degradation of the magnets over time. Alternatively, embedding PMs in the stator has been proposed to eliminate these mechanical stresses while also offering improved thermal management [3], [4]. Moreover, stator-PM machines, due to their high operating speeds, are suitable for direct-drive systems [5], [6].

Stator-PM motors are classified based on either PM arrangements or armature current type into four main categories: flux reversal PM (FRPM), flux switching PM (FSPM) [2], [5], [6], and doubly salient PM (DSPM) motors, all with sinusoidal excitation [7], [8], and finally PM-assisted switched reluctance motors (PMaSRMs) with square-wave voltages [9]. Although SRMs have a robust structure, they require non-conventional motor drives, increasing costs, high torque ripple, and low torque density [10], [11].

In contrast, FRPM, FSPM, and DSPM motors can operate with a standard three-phase inverter [12]. DSPMs produce lower torque and exhibit higher torque ripple compared to FSPM and FRPM [2], [5], [6] [13], [14]. In conventional FRPMs, PMs are mounted on the stator's surface. Considering the NdFeB PM permeability to be the same as air, the flux reversal array results in a higher air gap length, decreasing the air gap flux density [15]. Consequent pole designs, in which half of the PMs (or nearly half of the PMs) are replaced with iron cores, provide a viable solution [16]. In this paper, we propose a modular CP motor utilizing a flux reversal PM array. With the same PM volume utilization, our proposed motor demonstrates improved torque characteristics, including higher average torque and reduced torque ripple. The performance of the proposed motor is compared with conventional FRPM and E-type multi-tooth FSPM motors to highlight its advantages in this study.

Compared to recent FRPM structures [17]–[19], the proposed FRPM simplifies the manufacturing process by introducing a modular topology, in which the stator consists of six separate modules. In contrast, most high-torque stator-PM motors, such as FSPMs [20] and conventional FRPMs [21], adopt unitary stator structures, leading to a more complex and challenging manufacturing process [22], [23].

In this paper, Section II introduces the methodology of the proposed motor design. Additionally, the benchmark motors are presented alongside the proposed structure for comparison. In Section III, the performance enhancement achieved through

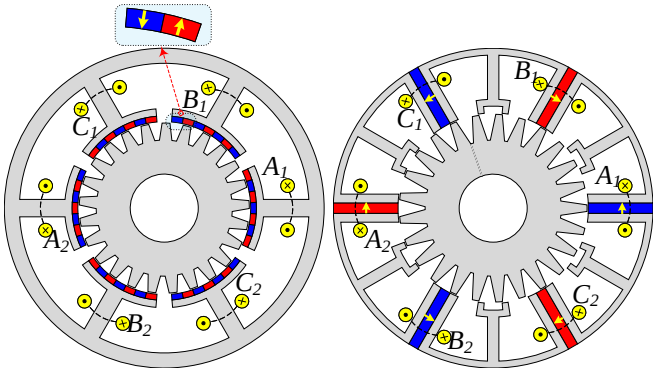

(a) (b)

Fig. 1. The structure of the conventional motors. (a) 25-rotor pole FRPM. (b) E-type multi-tooth FSPM.

TABLE I
MOTORS' BASIC SPECIFICATIONS

Specification	Proposed CPFRPM	FRPM	FSPM
Current density (A/mm^2)	6		
Frequency (Hz)	166.67		
Speed (rpm)	400		
Core material (Knee point)	M470-50 (1.6T)		
PM material	NdFeB-N42		
Cooling method	Natural convection		
PM volume (cm^2)	7		
Sizing parameters			
Shaft radius (mm)	10		
Stator outer radius (mm)	47		
Stack length (mm)	20		
Air gap length (mm)	0.4		

the novel PM arrangement is analyzed using a simplified magnetic equivalent circuit (MEC), and the optimization process is described in detail. Section IV highlights the advantages of the proposed motor based on finite element analysis (FEA) results. Finally, Section V outlines the prototyping plan and provides a comprehensive conclusion.

II. METHODOLOGY

The conventional FRPM and FSPM motors are shown in Figs. 1a and 1b, respectively. The conventional stator-PM motors suffer from a high risk of demagnetisation, which can be detailed as follows.

1) In the conventional FRPM machine, PMs are mounted on the stator pole tips. This PM pattern places the armature flux in series with the PM flux, resulting in a higher risk of demagnetisation.
2) In the FSPM motor, the PMs are sandwiched by the armature coils, which are the main source of heat in the motor. As a result, the PMs are exposed to high temperatures, leading to a higher risk of demagnetisation.

The proposed structure is obtained by deploying the modularity of the FSPM machine and the flux reversal effect of FRM, in which the PMs are radially magnetised (in the same direction) and are positioned in teeth intervals and slot openings. This PM arrangement leads to the integration of

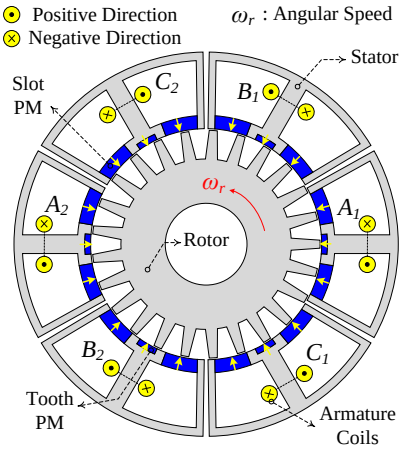

(a)

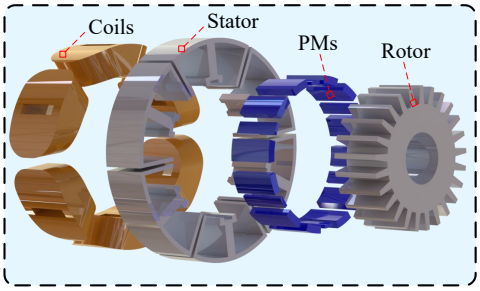

(b)

Fig. 2. (a) Proposed CPFRM. (b) Exploded view of the proposed structure.

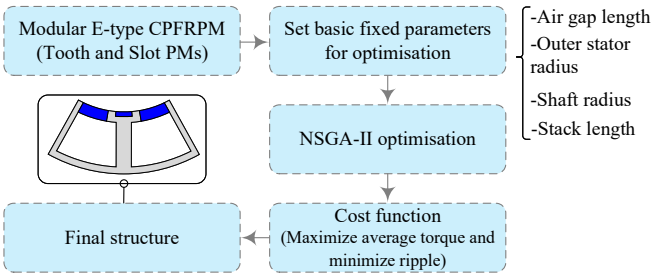

Fig. 3. The flowchart of methodology.

the CP-PM array into the proposed structure. The proposed motor reduces the demagnetisation risk by paralleling the PM flux with the armature coil flux. Consequently resulting in an improved air gap flux density and higher torque production. The proposed CP flux reversal motor (CPFRM) with a modular topology is shown in Fig. 2. The key design parameters of the motors are the same, including the outer stator radius (47 mm), PM volume (7 cm^3), stack length (20 mm), speed (400 rpm), current density (6 A/mm^2), and air gap length (0.4 mm). Other main parameters of the motors are listed in Table I.

Furthermore, the methodological procedure for obtaining the optimised structure of the CPFRPM is illustrated in Fig. 3. The fundamental design parameters, listed in Table I, are kept constant to ensure a fair comparative analysis. The Non-dominated Sorting Genetic Algorithm II (NSGA-II) is

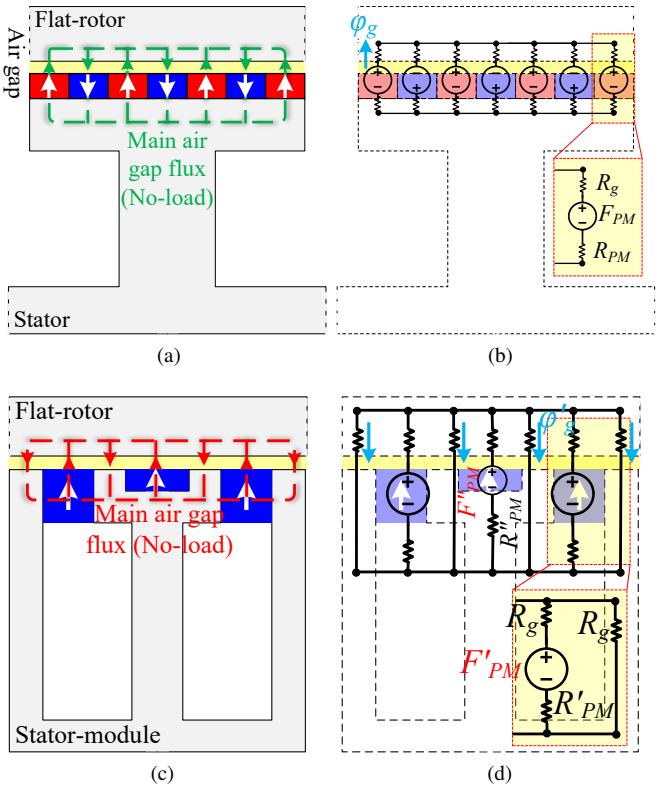

Fig. 4. (a) Simplified view and (b) MEC of FRPM. (c) Simplified view and (d) MEC of the proposed CPFRM.

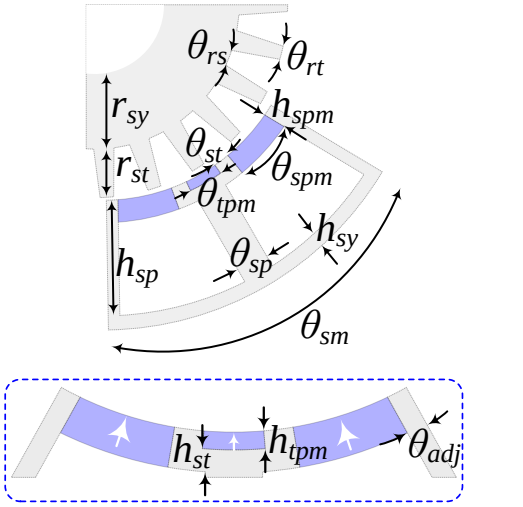

Fig. 5. Optimisation parameters of the proposed CPFRM.

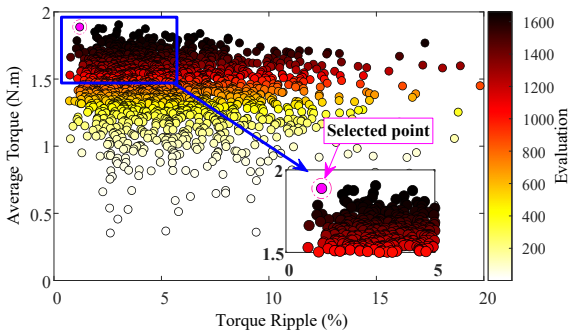

Fig. 6. Optimisation process of the proposed CPFRM.

employed to optimise the motor topology in conjunction with other stator-PM motor benchmarks.

III. Air Gap Magnetic Flux Enhancement and Optimisation

In this section, by comparing the proposed CPFRM and FRPM topologies, it is presented that the air gap flux is improved. Leading to better no-load and full-load performances. One-sixth of the conventional FRPM under no load and its MEC are shown in Fig. 4. The simplified MECs for the motors are considered with an ideal core and a flat rotor.

In the conventional FRPM structure, the air gap flux (φ_g) can be obtained as:

$$\varphi_g = \frac{F_{PM}}{R_g + R_{PM}}. \tag{1}$$

Also, one module of the proposed CPFRM and its simplified MEC are demonstrated in Fig. 4. The air gap flux of the proposed motor (φ'_g) is calculated in (2).

$$\begin{aligned}\varphi'_g = &\frac{2F'_{PM}}{R_T} \times \frac{5R_g + R''_{PM} + R'_{PM}}{6R_g + R''_{PM} + R'_{PM}} \\ &+ \frac{F''_{PM}}{R'_T} \times \frac{5R_g + 2R'_{PM}}{6R_g + 2R'_{PM}}\end{aligned} \tag{2}$$

where R_T and R'_T represent the equivalent reluctances and are given by the expression in (3) and (4).

$$\begin{aligned}R_T = &\underbrace{\left(\frac{R_g}{4} \parallel (R_g + R'_{PM}) \parallel (R_g + R''_{PM})\right)}_{\ll R_g} \\ &+ R_g + R'_{PM} \simeq R_g + R'_{PM},\end{aligned} \tag{3}$$

$$\begin{aligned}R'_T = &\underbrace{\left(\frac{R_g}{4} \parallel \frac{(R_g + R'_{PM})}{2}\right)}_{\ll R_g} + R_g + R''_{PM} \\ &\simeq R_g + R''_{PM}.\end{aligned} \tag{4}$$

By considering the volume of PMs, the equations for the magnetomotive forces (MMFs) and reluctances values are presented in (5). With these simplifications, the air gap magnetic flux of the proposed machine (φ'_g) is enhanced compared to the conventional one (φ_g), as shown in (5) and (6). By substituting the exact values of the MEC into equation (5), the air gap flux density demonstrates a 3.5-fold improvement compared to the conventional FRPM.

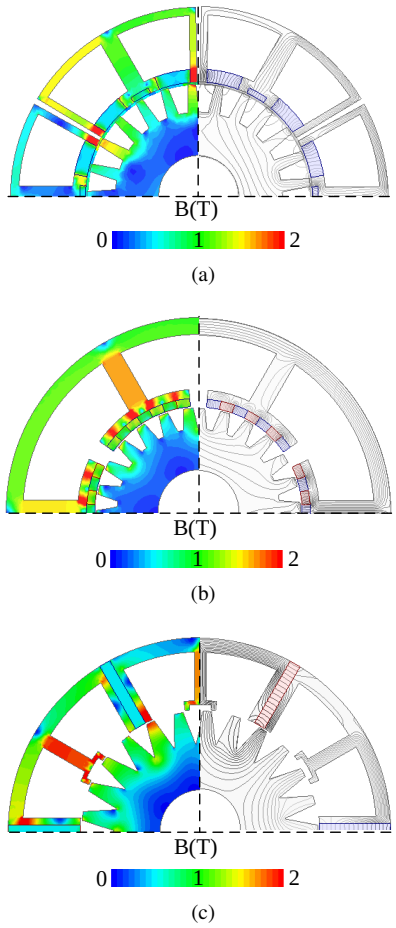

Fig. 7. Full-load flux density distributions: (a) Proposed. (b) FRPM. (c) FSPM.

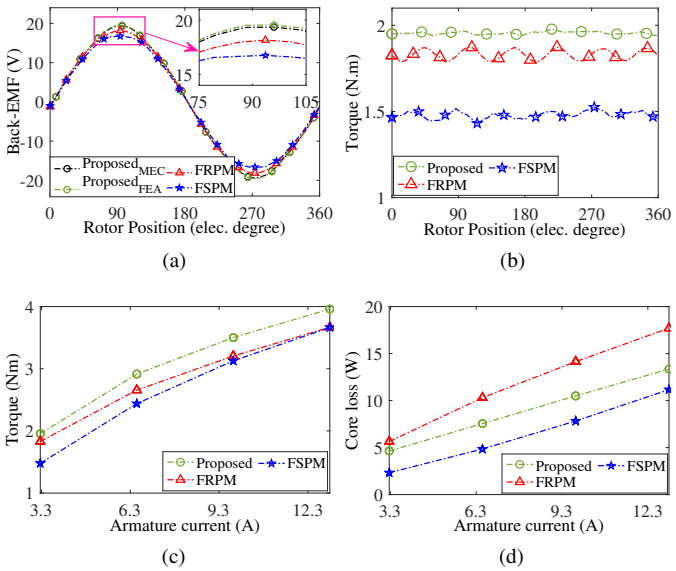

Fig. 8. (a) Back-EMF waveforms. (b) Full-load torque profile. (c) Overload torque profile. (d) Average core loss.

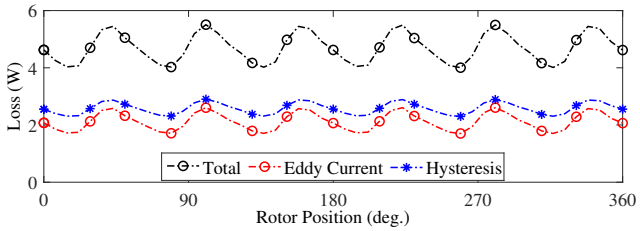

Fig. 9. Steady-state core loss distribution for the proposed motor.

$$\left.\begin{array}{l} R_{PM} \simeq 0.7{R'}_{PM} \simeq 0.5{R''}_{PM} \\ 7F_{PM} \simeq 1.75 \times (2{F'}_{PM} + {F''}_{PM}) \end{array}\right\}$$
$$\rightarrow {\varphi'}_g = \frac{4F_{PM} \times (5R_g + 3.4R_{PM})}{(R_g + 1.5R_{PM}) \times (6R_g + 3.4R_{PM})} \simeq 3.5\varphi_g \tag{5}$$

$$ {\varphi'}_g > \varphi_g \tag{6}$$

The proposed structure is optimised using a combination of FEA and Genetic Algorithm optimisation (GA). This optimisation configuration aims to maximise output torque while minimising torque ripple. The analysis is done on over 1500 samples with various optimisation variables, which is shown in Fig. 5. As illustrated in Fig. 6, we choose the optimal structure with the lowest cost function in the Pareto front. The cost function is defined as shown in (7).

$$\text{Cost Function} = M - \left(ATC \times \frac{T_{avg}}{DAT} + TRC \times \frac{DTR}{T_{ripple}} \right) \tag{7}$$

In (7), M, ATC, TRC, DAT, and DTR represent the cost function margin, the average torque coefficient, the torque ripple coefficient, the desired average torque, and the desired torque ripple, respectively. Also, T_{avg} and T_{ripple} represent the average torque and torque ripple values measured in each simulated sample. Also, this optimisation process is conducted to ensure that both conventional structures have a fair comparison. Also, the Pareto-front of the optimisation results is selected according to low torque ripple and high average torque. The coupled FEA and NSGA-II optimisation process aims to minimise the cost function value.

IV. Finite Element Analysis Results

In this section, the proposed CPFRM is compared with the conventional FRPM and E-type FSPM using finite element analysis (FEA). The flux density distributions and flux lines of the motors are illustrated in Fig. 7 under full load conditions. Fig. 7a exhibits the proposed CPFRM with smaller saturated regions and a lower saturation risk compared to the conventional motors shown in Figs. 7b and 7c, resulting in improved overload performance.

In terms of back-EMF, as shown in Fig. 8a, the maximum values of the sinusoidal curves for the proposed CPFRM, FRPM, and FSPM are 19.55V, 18.15V, and 16.75V, respectively. Additionally, Fig. 8b shows the CPFRM with a 7.1%

TABLE II
COMPARISON OF FEA RESULTS

Parameter	Proposed	FRPM	FSPM
Max. Back-EMF (V)	**19.55**	18.15	16.75
Torque (N.m)	**1.96**	1.83	1.47
PM torque density (N.m/L)	**277**	264	210
Torque ripple (%)	**2.1**	4.7	6.3
Core loss (W)	4.63	5.64	2.32
Copper loss (W)	4.23	4.23	4.23
Efficiency (%)	**90.2**	88.5	90

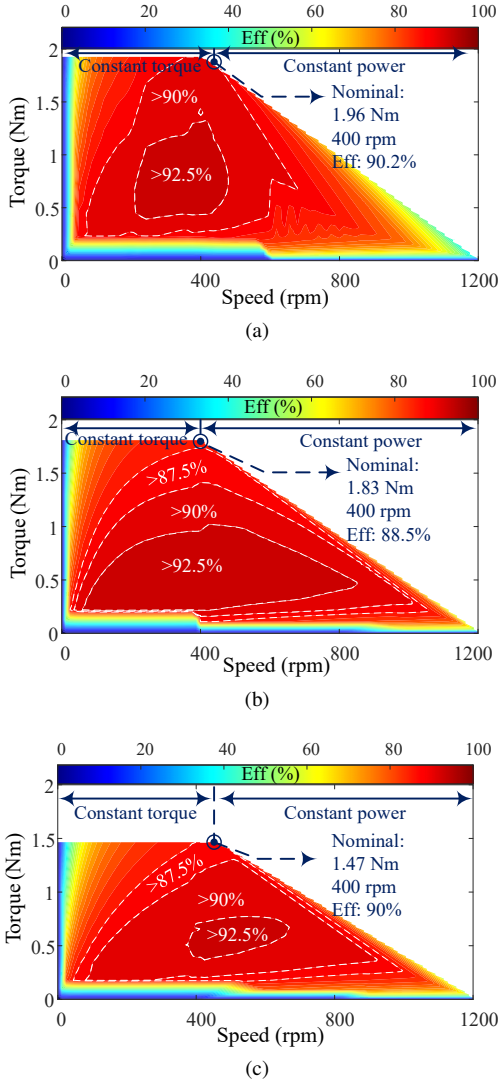

Fig. 10. Efficiency maps of the motors: (a) Proposed. (b) FRPM. (c) FSPM.

and 33.3% improvement in torque compared to the conventional FRPM and FSPM, respectively. The proposed CPFRM delivers an average torque value of 1.96Nm and a torque ripple of 2.1%, with 277 Nm/L PM torque density. For the first time, a motor of this compact size boasts an impressive torque density, setting a new benchmark.

For the overload performance of the motors, the CPFRM outperforms the conventional designs in terms of maximum torque under all armature currents, as shown in Fig. 8c. The

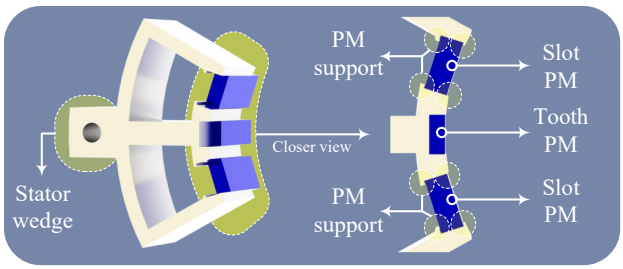

(a)

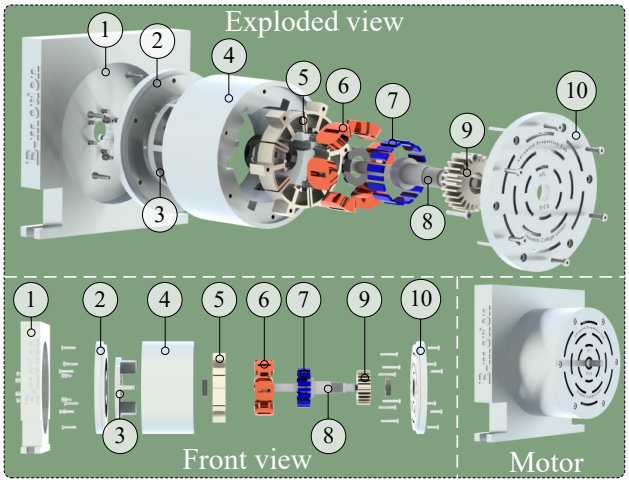

(b)

Fig. 11. Prototyping procedure. (a) One stator module. (b) Exploded view of the proposed motor: 1) Stand, 2) end cap, 3) leveler, 4) house, 5) stator, 6) coils, 7) PMs, 8) shaft, 9) rotor, 10) end cap.

average steady-state core losses of the motors are presented in Fig. 8d. At nominal current, the proposed CPFRM reduces core loss by approximately 18% compared to the FRPM. The efficiencies of the proposed CPFRM, FRPM, and FSPM are 90.2%, 88.5%, and 90%, respectively (see Table II for more details). It is worth noting that the core loss distribution of the motor is shown in Fig. 9. As can be seen, the core loss consists mainly of two components, eddy current loss and hysteresis loss, which have nearly equal values and were obtained through FEA. Fig. 10 presents the efficiency maps of the motors. The proposed CPFRPM exhibits the highest efficiency at nominal operating conditions. Moreover, it possesses a high-efficiency region that is 1.5 times larger than that of the FSPM, making it a promising candidate for EV applications.

The feasibility of the manufacturing procedure of CPFRPM is illustrated in Fig. 11. As mentioned in the introduction, one of the modules of the motor has been prototyped with considerations such as supports for slot and tooth PMs (see Fig. 11a). Moreover, the exploded view of the proposed motor, along with descriptions of each part, is shown in Fig. 11b.

V. CONCLUSION

In this paper, a new consequent pole flux reversal motor (CPFRM) with a modular stator was proposed. The improvement in the air gap flux compared to the conventional FRPM

was demonstrated through a MEC analysis validated by FEA. Additionally, the proposed CPFRM outperformed conventional FRPM and FSPM motors in terms of full-load torque, showing improvements of 7.1% and 33.3%, respectively. The torque ripple of the proposed CPFRM motor was reduced by 55.3% and 66.6% compared to the FRPM and FSPM, respectively. Furthermore, the proposed CPFRM achieved an efficiency of 90.2%. By analysing the overload conditions and flux density distributions, it was reported that the proposed motor exhibited better overload performance. In addition, the efficiency maps of the motors are analyzed to evaluate the performance of the proposed motor across various speed and torque operating points. The summary of the electromagnetic results was presented in Table II, demonstrating that the proposed CPFRM outperformed the two benchmark motors.

REFERENCES

[1] Q. Wang, X. Zhao, and S. Niu, "Flux-modulated permanent magnet machines: Challenges and opportunities," *World Electric Vehicle Journal*, vol. 12, no. 1, 2021. [Online]. Available: https://www.mdpi.com/2032-6653/12/1/13

[2] M. R. Sarshar, M. A. Jalali Kondelaji, P. Asef, and M. Mirsalim, "Electromagnetic investigation of innovative stator–permanent magnet motors," *Energies*, vol. 18, no. 9, p. 2400, 2025.

[3] J. Dong, Y. Huang, L. Jin, and H. Lin, "Comparative study of surface-mounted and interior permanent-magnet motors for high-speed applications," *IEEE Transactions on Applied Superconductivity*, vol. 26, no. 4, pp. 1–4, 2016.

[4] M. Amirkhani, M. A. J. Kondelaji, A. Ghaffarpour, M. Mirsalim, and S. Vaez-Zadeh, "Study of boosted toothed biased flux permanent magnet motors," *IEEE Transactions on Transportation Electrification*, vol. 8, no. 2, pp. 2549–2564, 2022.

[5] S. Cai, J. L. Kirtley, and C. H. T. Lee, "Critical review of direct-drive electrical machine systems for electric and hybrid electric vehicles," *IEEE Transactions on Energy Conversion*, vol. 37, no. 4, pp. 2657–2668, 2022.

[6] M. R. Sarshar, M. A. Jalali Kondelaji, P. Asef, and M. Mirsalim, "New multi-tooth inter-modular flux reversal permanent magnet motor," in *Japanese Society of Automove Engineering*. Japanese Society of Automove Engineering (JSAE), 2025.

[7] H. Yang, Y. Li, H. Lin, Z. Q. Zhu, and S. Lyu, "Principle investigation and performance comparison of consequent-pole switched flux pm machines," *IEEE Transactions on Transportation Electrification*, vol. 7, no. 2, pp. 766–778, 2021.

[8] Y. Liao, F. Liang, and T. Lipo, "A novel permanent magnet motor with doubly salient structure," *Industry Applications, IEEE Transactions on*, vol. 31, pp. 1069 – 1078, 10 1995.

[9] M. Masoumi and M. Mirsalim, "E-core hybrid reluctance motor with permanent magnets inside stator common poles," *IEEE Transactions on Energy Conversion*, vol. 33, no. 2, pp. 826–833, 2017.

[10] T. Miller, *Switched Reluctance Motors and Their Control*, ser. Monographs in electrical and electronic engineering. Magna Physics, 1993. [Online]. Available: https://books.google.co.uk/books?id=wK5UngEACAAJ

[11] M. Amirkhani, M. A. Ghanbari, M. A. J. Kondelaji, M. Mirsalim, and A. Khorsandi, "Performance analysis of outer rotor multi-tooth biased flux permanent magnet motors," *IEEE Transactions on Energy Conversion*, vol. 38, no. 3, pp. 1738–1752, 2023.

[12] H. Yang, Z. Q. Zhu, H. Lin, H. Li, and S. Lyu, "Analysis of consequent-pole flux reversal permanent magnet machine with biased flux modulation theory," *IEEE Transactions on Industrial Electronics*, vol. 67, no. 3, pp. 2107–2121, 2020.

[13] Y. Liao, F. Liang, and T. Lipo, "A novel permanent magnet motor with doubly salient structure," *IEEE Transactions on Industry Applications*, vol. 31, no. 5, pp. 1069–1078, 1995.

[14] J. Zhang, M. Cheng, Z. Chen, and W. Hua, "Comparison of stator-mounted permanent-magnet machines based on a general power equation," *IEEE Transactions on Energy Conversion*, vol. 24, no. 4, pp. 826–834, 2009.

[15] Y. Zheng, W. Xiang, H. Xu, P. Tan, and Y. Fang, "Analysis of a flux reversal machine with consequent-pole evenly distributed pm," *IEEE Transactions on Industry Applications*, vol. 60, no. 1, pp. 4–11, 2024.

[16] F. Wei, Z. Q. Zhu, X. Sun, L. Yan, and J. Qi, "Investigation of asymmetric consequent-pole hybrid excited flux reversal machines," *IEEE Transactions on Industry Applications*, vol. 58, no. 3, pp. 3434–3446, 2022.

[17] K. Yang, F. Zhao, Y. Wang, and Z. Bao, "Consequent-pole flux reversal permanent magnet machine with halbach array magnets in rotor slot," *IEEE Transactions on Magnetics*, vol. 57, no. 2, pp. 1–5, 2021.

[18] K. Xie, D. Li, R. Qu, Z. Yu, Y. Gao, and Y. Pan, "Analysis of a flux reversal machine with quasi-halbach magnets in stator slot opening," *IEEE Transactions on Industry Applications*, vol. 55, no. 2, pp. 1250–1260, 2019.

[19] H. Hua and Z. Q. Zhu, "Investigation on symmetrical characteristics of consequent-pole flux reversal permanent magnet machines with concentrated windings," *IEEE Transactions on Energy Conversion*, vol. 37, no. 3, pp. 1815–1824, 2022.

[20] Y. Bi, W. Fu, S. Niu, X. Zhao, and J. Huang, "Design of a dual-set permanent magnet flux-switching machine with enhanced torque density and fault-tolerance capability," *IEEE Transactions on Transportation Electrification*, pp. 1–1, 2023.

[21] R. Deodhar, S. Andersson, I. Boldea, and T. Miller, "The flux-reversal machine: a new brushless doubly-salient permanent-magnet machine," *IEEE Transactions on Industry Applications*, vol. 33, no. 4, pp. 925–934, 1997.

[22] W. Ouyang and T. A. Lipo, "Modular permanent magnet machine with fault tolerant capability," in *2009 Twenty-Fourth Annual IEEE Applied Power Electronics Conference and Exposition*, 2009, pp. 930–937.

[23] N. Bianchi, S. Bolognani, M. Pre, and G. Grezzani, "Design considerations for fractional-slot winding configurations of synchronous machines," *IEEE Transactions on Industry Applications*, vol. 42, no. 4, pp. 997–1006, 2006.